Ferrioxalate-assisted solar photo-Fenton degradation of a herbicide at pH conditions close to neutrality

Leandro O. Conte, Agustina V. Schenone & Orlando M. Alfano

Environmental Science and Pollution Research

ISSN 0944-1344
Volume 24
Number 7

Environ Sci Pollut Res (2017)
24:6205-6212
DOI 10.1007/s11356-016-6400-3

Springer

Environ Sci Pollut Res (2017) 24:6205–6212
DOI 10.1007/s11356-016-6400-3

Ferrioxalate-assisted solar photo-Fenton degradation of a herbicide at pH conditions close to neutrality

Leandro O. Conte[1] · **Agustina V. Schenone**[1] · **Orlando M. Alfano**[1]

Received: 27 November 2015 / Accepted: 1 March 2016 / Published online: 14 March 2016

Abstract The solar photo-Fenton degradation of the herbicide 2,4-dichlorophenoxyacetic acid (2,4-D) in aqueous solution at a natural pH (pH = 5) using ferrioxalate as iron source was investigated. The kinetic model proposed and validated in a previous contribution was used to predict the reactants concentrations during the oxidation process in a non-concentrating pilot-plant solar reactor. The effects of hydrogen peroxide to 2,4-D initial concentration ratios (*R*), temperature, and radiation levels were studied. Furthermore, the spectral UV/visible and broadband solar radiation fluxes incident on the reactor window were evaluated by the Simple Model for the Atmospheric Radiative Transfer of Sunshine (SMARTS2) code. The complete destruction of 2,4-D and its main intermediate 2,4-dichlorophenol (2,4-DCP) was achieved in all the experimental runs in only 90 and 120 min of reaction, respectively. In agreement with these results, a reduction of toxicity in the system (expressed as % of inhibition of *Vibrio fischeri*) for longer times to 90 min of reaction was attained. It is important to emphasize the good agreement between kinetic model results and experimental data obtained.

Keywords 2,4-D · Ferrioxalate · Neutral pH · Solar photo-Fenton

Responsible editor: Bingcai Pan

✉ Orlando M. Alfano
alfano@intec.unl.edu.ar

[1] Instituto de Desarrollo Tecnológico para la Industria Química (INTEC), Consejo Nacional de Investigaciones Científicas y Técnicas (CONICET) and Universidad Nacional del Litoral (UNL), Ruta Nacional N°168, 3000 Santa Fe, Argentina

Introduction

The Fenton reaction is one of the advanced oxidation processes (AOPs) which involves the generation of hydroxyl radical (OH·), a non-selective oxidizing agent, by interaction of hydrogen peroxide (HP) with ferrous salts in acidic medium. This highly reactive species promotes the oxidation of hazardous organic compounds. Fenton reaction can be accelerated by irradiation with UV light, which is known as the photo-Fenton reaction. The UV radiation improves the efficiency of the process due principally to the photochemical reduction of Fe(III) back to Fe(II). This reaction also produces an additional hydroxyl radical (Pignatello et al. 2006).

In order to avoid iron precipitation, the photo-Fenton process is carried out in acidic medium, typically at pH 2.8 (Malato et al. 2009). At this value, predominant Fe(III) species present in aqueous solution is $Fe(OH)^{2+}$, which mainly absorbs radiation in the ultraviolet spectral region. An approach to avoid acidification and ferric iron hydroxide precipitation is to perform the reaction with complexing agents, especially with organic compounds (Conte et al. 2014; De Lima Perini et al. 2013). Furthermore, these complexes usually have higher molar absorption coefficients in the near-UV and visible spectra when compared to mono- and di-hydroxylated complexes of Fe(III) (Malato et al. 2009). Among the many ligands, oxalate has been widely applied in order to stabilize iron in solution at near-neutral pH conditions in the treatment of polluted water (Hislop and Bolton 1999; Schenone et al. 2015; Soares et al. 2015).

Recently, solar technology has transformed the photo-Fenton process into a non-expensive and competitive method for the chemical destruction of organic pollutants. The use of

solar reactors is an interesting option for the treatment of effluents, with some benefits such as elimination of costs associated with installation and maintenance of UV lamps and with electrical power consumption (Nascimento et al. 2007). The specific literature has reported the application of the solar photo-Fenton process for the remediation of waters containing toxic and non-biodegradable organic contaminants, e.g., persistent pharmaceutical compounds (Miralles-Cuevas et al. 2015; Radjenovic et al. 2009), pesticides (Conte et al. 2012; Navarro et al. 2011;), textile effluents (Pérez et al. 2002), non-biodegradable dyes (Monteagudo et al. 2009), cellulose bleaching effluents (Lucas et al. 2012), and real effluents from municipal treatment plants (Klamerth et al. 2010).

Different designs of solar reactors have been proposed in recent years in order to conduct photochemical processes. Both concentrating (several-suns) and non-concentrating (one-sun) collectors have been adopted in the design and construction of solar reactors for an efficient utilization of the solar radiation at the Earth's surface. Their advantages and disadvantages have been compared and discussed (Alfano et al. 2000; Malato et al. 2009; Parra et al. 2001). It is known that one-sun reactors can absorb both direct and diffuse sun irradiation that arrives at ground level, whereas concentrating devices are only able to collect the direct radiation (Bockelman et al. 1995; Ollis 1991).

In a previous study, the degradation of herbicide 2,4-dichlorophenoxyacetic acid (2,4-D) was investigated using the ferrioxalate complex as iron source, for conditions of pH close to neutrality and operating the system under simulated solar radiation (Conte et al. 2016). The effects of the variables: reaction temperature (T) and HP to 2,4-D initial concentration ratio (R) were also evaluated. A kinetic model derived from a reaction sequence was also proposed, and the associated parameters were estimated applying a non-linear regression method. In the present work, the mentioned validated model is used to evaluate temporal variations of 2,4-D, the main intermediate 2,4-dichlorophenol (2,4-DCP), and hydrogen peroxide concentrations in a pilot-plant solar reactor. In this case, it is necessary to solve simultaneously the mass and thermal energy balances and simulate the solar radiation (direct and diffuse) that reaches the reactor window. This last step is achieved with the aid of a computational code: the Simple Model for the Atmospheric Radiative Transfer of Sunshine (SMARTS2) program (Conte et al. 2012). The predicted species concentrations as a function of time were compared with the experimental values.

Regarding the contaminant employed in this study, 2,4-D is the active ingredient in several formulations of herbicides and it is the second most used herbicide in Argentina. It is known that the inadequate management of pesticides can cause contamination of the soil and of subterranean and surface water sources. In the specific literature, several AOPs have been proposed to remove 2,4-D from aqueous samples (Alfano et al. 2001; Conte et al. 2012; Kwan and Chu 2004; Schenone et al. 2015).

Finally, since the degradation of organic pollutants by the hydroxyl radical can lead to by-products that can be more toxic than the original contaminant, the Microtox® test was employed during the photo-Fenton treatment. Therefore, the bioluminescence of the bacteria *Vibrio fischeri* was followed as a function time.

Experimental

Experimental device

The solar experimental runs were performed in a pilot-plant solar reactor placed inside a batch recycling system that has a high-flow-rate centrifugal pump and a storage tank. This non-concentrating solar photoreactor is able to capture the UV/visible and near-infrared solar radiation (Fig. 1). The solution to be treated enters in a lower channel of the reactor where it is preheated. Then, the fluid circulates into an upper channel where it is further heated, absorbs the UV/visible solar radiation, and makes use of this absorbed radiation for the pollutants degradation. The total volume of the treated solution was 35 L, while the irradiated reactor volume (Virr) was 6.1 L. The reactor depth, window area (Aw), and plate thickness were 30 mm, 0.24 m^2, and 3.2 mm, respectively. More details of the reactor configuration can be found elsewhere (Conte et al. 2012; Farias et al. 2010).

Procedure

Each experimental run starts when 2,4-D (Aldrich, 98 %) and ferric oxalate solutions are added to the storage tank. At the beginning of the experimental runs, the reactor window was covered with an opaque plate to avoid the entrance of solar radiation. The iron complex solution was prepared following the methodology described by Murov et al. (1993), using potassium oxalate monohydrate (Carlo Erba, 99.5 %) and $FeCl_3 \cdot 6H_2O$ (Merck). In all cases, the medium pH is adjusted to 5 with a concentrated solution of sodium hydroxide (1.0 mol L^{-1}, Cicarelli). Finally, hydroxide peroxide solution is added (Carlo Erba, ACS, 30 %). Immediately, the first sample is taken and then the reactor cover removed to start the solar reaction. The progress of the reaction was monitored for 120 min.

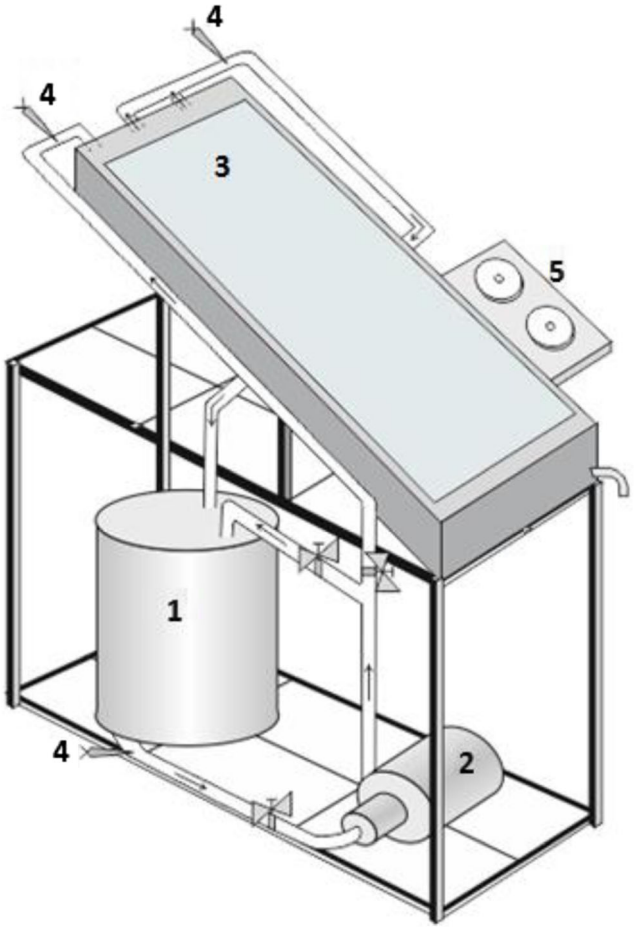

Fig. 1 Scheme of the solar pilot-plant reactor. (*1*) Storage tank, (*2*) recirculation pump, (*3*) photoreactor, (*4*) thermocouples, and (*5*) radiometers

For all tests, the 2,4-D initial concentration was 0.136 mM (30 mg L^{-1}), the initial iron concentration was 0.054 mM (3 mg L^{-1}), and the initial oxalate ion concentration was 0.54 mM. Different HP/2,4-D molar ratios (*R*) on the photo-Fenton process were investigated.

During the experimental runs, the UV and total broadband solar radiation fluxes incident on the reactor window were measured by CUV3 and CM11 Kipp and Zonen radiometers. Reactor temperatures were monitored with thermocouples type J in different positions of the reactor. In order to improve the quality/quantity of the collected data associated with the behavior of the solar reactor (temperature, UV and total radiation, and pH), a data acquisition board was built. It allows the on-line recording of the variables mentioned before, in time intervals in the order of seconds.

Analytical methods

The samples used to determine 2,4-D and 2,4-DCP were pretreated with methanol (Sintorgan, grade HPLC) in order to stop the reaction. HPLC (Waters) with UV-vis detector was used to monitor 2,4-D and 2,4-DCP concentrations using an LC-18 Supelcosil reverse phase column (Supelco) and a mobile phase prepared with a mixture of ultrapure water, acetonitrile, and anhydrous acetic acid (45:50:5). Sodium sulfite was used in the pretreatment step of the samples for total organic carbon (TOC) determination using a Shimadzu TOC-5000A analyzer. A UV-vis CARY 100 BIO spectrophotometer was used for both HP and total Fe determinations. In the case of HP, a modified iodometric technique was applied; the measurement was done at 350 nm. Samples for iron determination were pretreated with ascorbic acid, and the analysis was done by means of the colorimetric method with 1,10-phenanthroline at 510 nm. Toxicity measurements were carried out throughout the photo-Fenton treatment. For this purpose, Microtox Model 500 Toxicity Analyser (Strategic Diagnostic Inc.) was used. Hydrogen peroxide was removed prior to analysis using catalase (1500 mg L^{-1} of >2000 U mg^{-1} bovine liver, Fluka), and the sample pH was adjusted between 6 and 8.

Preliminary studies

Neutral pH conditions are usually found in contaminated wastewater. Therefore, it is important to investigate the feasibility of applying the photo-Fenton process for pH conditions close to neutrality.

Since iron solubility strongly decreases with increasing pH, the ferrioxalate complex was studied as an iron source for the process at pH conditions close to 5 (Conte et al. 2012). This pH is the naturally found value in an effluent where 2,4-D is dissolved (concentrations ranging from 20 to 30 mg L^{-1}). For this purpose, the iron-oxalate system speciation was evaluated for different molar concentration ratios of oxalate/iron (Ox/Fe). The adopted molar concentration ratio of oxalate/iron (Ox/Fe) in this work was 10 (greater than the stoichiometric ratio Ox/Fe = 3). It was demonstrated that iron precipitation was avoided using this oxalate/iron ratio. Moreover, under operating conditions of pH = 5 and Ox/Fe = 10, a molar fraction close to 90 % of $Fe^{(III)}(C_2O_4)_3^{3-}$ was reached (Conte et al. 2016). Besides, this complex absorbs radiation in the UV-visible region more efficiently than the aqueous complexes found in the standard Fenton system (De Souza et al. 2013).

From the previous comments, a kinetic model derived from a simplified reaction sequence using ferrioxalate as iron source and conditions of pH = 5 was proposed (see

Table 1 Simplified reaction scheme of 2,4-D photo-Fenton degradation and optimized kinetic parameters

Number	Reaction step	Optimized kinetic parameters	Units
0	$Fe^{(III)}(C_2O_4)_3^{3-} \rightarrow^{h\nu} Fe^{(II)}(C_2O_4) + CO_2 + 1.5C_2O_4^{2-}$	$\overline{\Phi}_{Fe^{(II)}(C_2O_4)} = 1.21$	mol E^{-1}
		$\overline{\Phi}_{C_2O_4^{2-}} = 1.05$	mol E^{-1}
1	$Fe^{(III)}(C_2O_4)_3^{3-} + H_2O_2 \rightarrow Fe^{(II)}(C_2O_4) + 2C_2O_4^{2-} + OH^{\bullet} + OH^{-}$	$A_1 = -2.76$ $B_1 = 4.37$	(–)
2	$Fe^{(II)}(C_2O_4) + H_2O_2 + 2C_2O_4^{2-} \rightarrow Fe^{(III)}(C_2O_4)_3^{3-} + OH^{\bullet} + OH^{-}$	$k_2 = 3.10 \times 10^4$	$M^{-1}\ s^{-1}$
3	$H_2O_2 + OH^{\bullet} \rightarrow O_2^{-\bullet} + H^{+} + H_2O$	$k_3 = 3.76 \times 10^7$	$M^{-1}\ s^{-1}$
4	$2,4\text{-D} + OH^{\bullet} \rightarrow 2,4\text{-DCP}$	$k_4 = 3.00 \times 10^9$	$M^{-1}\ s^{-1}$
5	$2,4\text{-DCP} + OH^{\bullet} \rightarrow \text{products}$	$k_5 = 2.38 \times 10^{10}$	$M^{-1}\ s^{-1}$
6	$C_2O_4^{2-} + OH^{\bullet} \rightarrow \text{products}$	$k_6 = 7.70 \times 10^6$	$M^{-1}\ s^{-1}$

Table 1). Here, the experimental runs were performed in a lab-scale flat plate reactor irradiated with a solar simulator (Conte et al. 2016).

The effect of the reaction temperature on the behavior of the system was evaluated from the Arrhenius equation (reaction N1, Table 1). Accordingly, k_1 was defined as $k_1 = \exp\left[A_1 + B_1\left(\frac{T-T_{ref}}{T}\right)\right]$, in which $A_1 = \ln(k_{ref,1}) = \ln(k_{\infty,1}) - E_1/\Re T_{ref}$ and $B_1 = E_1/\Re T_{ref}$. In which $k_{ref,1}$ is the kinetic constant for reaction N1 associated to the reference temperature (T_{ref}= 298 K), $k_{\infty,1}$ is the specific reaction constant at infinite temperature, E_1 is the activation energy, and $\Re$ is the universal constant of ideal gases.

Among the constants listed in Table 1, only k_3, k_5, $\overline{\Phi}_{Fe^{(II)}(C_2O_4)}$ and $\overline{\Phi}_{C_2O_4^{2-}}$ were estimated/optimized simultaneously within the minimum and maximum values found in the specific literature. For this purpose, a Newton Gauss-Marquardt algorithm was used. The remaining parameters were taken from the literature (Conte et al. 2016).

Therefore, the reaction rates expressions obtained for 2,4-D, 2,4-DCP, HP, and Ox by considering the simplified scheme shown in Table 1 are presented below.

$$\begin{bmatrix} R_{2,4\text{-D}}(x,t) \\ R_{2,4\text{-DCP}}(x,t) \\ R_{Fe^{(II)}(C_2O_4)}(x,t) \\ R_{Fe^{(III)}(C_2O_4)_3^{3-}}(x,t) \\ R_{HP}(x,t) \\ R_{C_2O_4^{2-}}(x,t) \end{bmatrix} = \begin{bmatrix} R^T_{2,4\text{-D}}(t) \\ R^T_{2,4\text{-DCP}}(t) \\ R^T_{Fe^{(II)}(C_2O_4)}(t) \\ R^T_{Fe^{(III)}(C_2O_4)_3^{3-}}(t) \\ R^T_{HP}(t) \\ R^T_{C_2O_4^{2-}}(t) \end{bmatrix} + \sum_{\lambda} e^a_{\lambda}(x,t) \begin{bmatrix} 0 \\ 0 \\ \overline{\Phi}_{Fe^{(II)}(C_2O_4)} \\ -\overline{\Phi}_{Fe^{(II)}(C_2O_4)} \\ 0 \\ -\overline{\Phi}_{C_2O_4^{2-}} \end{bmatrix} \quad (1)$$

Note that Eq. 1 for the six reacting species can be also written by using the following matrix representation:

$$\mathbf{R}(x,t) = \mathbf{R}^T(t) + \mathbf{\Phi}\sum_{\lambda} e^a_{\lambda}(x,t) \quad (2)$$

The first term on the right-hand side of Eq. 1 or 2, which corresponds to the thermal reaction rate, may be represented by the matrix expression:

$$\begin{bmatrix} R^T_{2,4\text{-D}}(t) \\ R^T_{2,4\text{-DCP}}(t) \\ R^T_{Fe^{(II)}(C_2O_4)}(t) \\ R^T_{Fe^{(III)}(C_2O_4)_3^{3-}}(t) \\ R^T_{HP}(t) \\ R^T_{C_2O_4^{2-}}(t) \end{bmatrix} = \begin{bmatrix} -k_4 C_{2,4\text{-D}} C_{OH^{\bullet}} \\ \left(k_4 C_{2,4\text{-D}} - k_5 C_{2,4\text{-DCP}}\right) C_{OH^{\bullet}} \\ \left(k_1 C_{Fe^{(III)}(C_2O_4)_3^{3-}} C_{HP} - k_2 C_{Fe^{(II)}(C_2O_4)} C_{HP}\right) \\ \left(-k_1 C_{Fe^{(III)}(C_2O_4)_3^{3-}} C_{HP} + k_2 C_{Fe^{(II)}(C_2O_4)} C_{HP}\right) \\ -k_3 C_{HP} C_{OH^{\bullet}} - \left(k_1 C_{Fe^{(III)}(C_2O_4)_3^{3-}} C_{HP} + k_2 C_{Fe^{(II)}(C_2O_4)} C_{HP}\right) \\ -k_6 C_{C_2O_4^{2-}} C_{OH^{\bullet}} \end{bmatrix} \quad (3)$$

where

$$C_{OH^{\bullet}} = \left[\frac{k_1 C_{Fe^{(III)}(C_2O_4)_3^{3-}} C_{HP} + k_2 C_{Fe^{(II)}(C_2O_4)} C_{HP}}{k_3 C_{HP} + k_4 C_{2,4\text{-D}} + k_5 C_{2,4\text{-DCP}} + k_6 C_{C_2O_4^{2-}}}\right] \quad (4)$$

Balance equations for solar reactor

The mass balances and initial conditions for the pilot-plant solar reactor are given by the following set of first-order, ordinary differential equations (in matrix notation):

$$\frac{d}{dt}\mathbf{C}(t) = \mathbf{R}^T(t) + \frac{V_{irr}}{V}\mathbf{\Phi}\left\langle \sum_{\lambda} e^a_{\lambda}(x,t) \right\rangle_{Virr} \quad (5)$$

$$\mathbf{C} = \mathbf{C}^0 \qquad t = 0 \quad (6)$$

Note that the required reaction rate expressions to be replaced in Eq. 5 are given by Eqs. 1, 3, and 4.

It is important to note that for the numerical evaluation of the second term on the right-hand side of Eq. 5, it is necessary to know the value of the local volumetric rate of photon absorption (LVRPA) at every point inside

the reactor and then to compute the LVRPA averaged over the reactor volume. The value of the LVRPA defined for monochromatic radiation can be obtained assuming that the reactor window is irradiated by direct beam ($e^a_{B,\lambda}$) and diffuse ($e^a_{D,\lambda}$) solar radiation. Thus, the spectral LVRPA for the total solar radiation is given by the following equations:

$$e^a_\lambda(x,t) = e^a_{B,\lambda}(x,t) + e^a_{D,\lambda}(x,t) \quad (7)$$

$$e^a_{B,\lambda}(x,t) = \kappa_\lambda(t)\, q_{B,\lambda}(t)\, Y_{B,\lambda}(\mu_i) \exp\left[-\kappa_{T,\lambda}(t)\, x/\mu_{ref}\right] \quad (8)$$

$$e^a_{D,\lambda}(x,t) = 2\kappa_\lambda(t)\, q_{D,\lambda}(t) Y_{D,\lambda}(\mu_i)\, E\left[\kappa_{T,\lambda}(t), x\right] \quad (9)$$

where $q_{B,\lambda}$ and $Y_{B,\lambda}$ are the spectral direct beam radiation flux and transmittance, $q_{D,\lambda}$ and $Y_{D,\lambda}$ are the spectral diffuse radiation flux and transmittance, κ_λ is the spectral volumetric absorption coefficient of the absorbing species, and $\kappa_{T,\lambda}$ is the total absorption coefficient of the reacting medium. Besides, μ_{ref} is the cosine of refraction angle, μ_i the cosine of incident angle, and $E(t,x)$ is the second-order exponential integral function (Siegel and Howell 2002). Further details related to the calculation of the different terms involved in Eqs. (8) and (9) can be found elsewhere (Conte et al. 2012).

Moreover, to solve Eqs. 8 and 9, it is considered that $Fe^{(III)}(C_2O_4)_3^{3-}$ is the dominant ferric species at pH close to 5, and that the radiation absorption of HP and complex ferrous iron is negligible for wavelengths greater than 300 nm. Consequently,

$$\kappa_{T,\lambda}(t) = \sum_i \alpha_{i,\lambda} C_i(t) \cong \alpha_{Fe^{(III)}(C_2O_4)_3^{3-},\lambda} C_{Fe^{(III)}(C_2O_4)_3^{3-}}(t) \quad (10)$$

In Eq. 10, the molar absorptivity of the main absorbing species ($\alpha_{Fe^{(III)}(C_2O_4)_3^{3-}}$) is a function of the wavelength λ. These coefficients were determined experimentally (Conte et al. 2014 and 2016).

Since the solar radiation and the optical properties of the reactants are functions of wavelengths, integration over all the useful wavelengths must be performed to compute $e^a(x,t)$:

$$e^a(x,t) = \int_{\lambda_{min}}^{\lambda_{max}} e^a_\lambda(x,t)\, d\lambda \cong \sum_\lambda e^a_\lambda(x,t) \quad (11)$$

It is important to emphasize that the solar reactor is able to capture the UV/visible and near-infrared solar radiation, yielding important temperature increases during an experimental run. This fact can be beneficial from the reactor performance point of view, due to the positive effects on the thermal (Fenton) reaction rate. Consequently, a thermal energy balance must be written and solved to evaluate these temperature increases.

So the thermal energy balance and the initial condition for a solar reactor placed inside the loop of a batch recycling system is given by the following equations:

$$\frac{d}{dt}T(t) = \Omega \mathrm{Acq}_T(t) - \Gamma[T - Ta(t)] + K \quad (12)$$

$$T = T^0 \qquad t = 0 \quad (13)$$

in which $\Omega = 9.10 \times 10^{-5}$ °C J^{-1}, $\Gamma = 5.39 \times 10^{-6}$ s^{-1}, and $K = 8.28 \times 10^{-4}$ °C s^{-1} are the thermal parameters associated with the operation of the experimental device (Conte et al. 2012).

Although q_T and Ta are usually a function of time, no significant temporal variation was experimentally observed during the course of the reaction (the run duration is equal to 2 h). This is associated with the fact that the tests were conducted during similar summer conditions and were initiated at the same local standard time.

Results and discussion

Experimental results

Table 2 presents the experimental runs that were performed in order to evaluate the degradation of 2,4-D in the pilot-plant solar reactor. Furthermore, the herbicide conversions are shown at 30 min ($X^{30}_{2,4\text{-D}}$) and 60 min ($X^{60}_{2,4\text{-D}}$), as well as the reached mineralization levels at 120 min (X^{120}_{TOC}).

As it can be seen, the obtained herbicide conversions are close to 100 % in just 60 min of reaction in the three experimental runs. On the other hand, the mineralization levels after 120 min present a maximum of only 73.8 % for condition of $R = 28.5$. At this point, it is considered appropriate to emphasize that, for the process under study, total mineralization of the system is not desired since it would imply the complete destruction of the ferrioxalate complex. This fact would limit the effectiveness of the process due to the consequent precipitation of iron. However, it is intended to destroy the reaction intermediates generated from degradation of the herbicide, since they influence the toxicity of the system (mainly 2,4-DCP).

Table 2 2,4-D conversions at different experimental conditions in the solar reactor*

Nº	R	$X^{30}_{2,4\text{-D}}$ (%)	$X^{60}_{2,4\text{-D}}$ (%)	X^{120}_{TOC} (%)
1	7	79.7	98.8	55.6
2	28.5	78.6	100	73.8
3	50	57.3	91.5	62.7

*The start time of the experiments was 12.0 LST

Model and experimental results

Since the mass and energy balances are coupled, a resolution procedure was performed in four steps: (i) calculation of the direct and diffuse solar radiation spectrum incident on the reactor window, (ii) computation of the spectral LVRPA (Eqs. 7–9), (iii) evaluation of the reaction rate associated to each reactive species (Eqs. 1, 3, and 4), and (iv) calculation of the temporal variations of the reactive species concentrations (Eqs. 5 and 6) and the reaction temperature (Eqs. 12 and 13).

The simulation of the total and UV/Vis solar radiation incident on the reactor was done with the SMARTS2 code. For this purpose, it was necessary to know or estimate atmospheric parameters present at the time of each of the experimental runs (Conte et al. 2012). Although direct and diffuse solar radiations are a function of time (by the variation of the solar zenith angle), their corresponding values at 60 min of reaction (LTS 13.0) were considered.

Table 3 presents the obtained increments of temperature ($t = 120$ min), the UV and total radiation level experimentally measured (q_{UV}^{exp} and q_{Tot}^{exp}), and the same parameters estimated by the SMARTS2 code (q_{UV}^{est} and q_{Tot}^{est}, $t = 60$ min). In addition, the incident total radiation flux q_{Tot}^{inc} (direct and diffuse radiation) over the reaction surface between 300 and 500 nm was presented.

Firstly, it is important to highlight the correct simulation results achieved for the atmospheric conditions present in each of the runs. This is demonstrated with the minimum differences found between the experimental values acquired with the radiometers and the estimated values of UV and total radiation. Furthermore, the calculated q_{Tot}^{inc} values are in the same order as those used in the lab-scale reactor which was applied by Conte et al. (2016).

Figure 2 shows model predictions and experimental data of the temporal evolutions of 2,4-D, 2,4-DCP, HP, and Ox concentrations for the runs shown in Table 3. For 2,4-D, HP, and Ox, the relative concentrations are defined using the corresponding initial concentration of each species, while for the 2,4-DCP, the initial concentration of 2,4-D was employed. In addition, the maximum experimental errors associated with the determinations of 2,4-D (7.28×10^{-4} mM), 2,4-DCP (8.65×10^{-4} mM), HP (1.97×10^{-1} mM for the range 0–2.94 mM HP and 2.52×10^{-1} mM for the range 2.94–8.82 mM HP), and Ox (3.19×10^{-2} mM) were presented (Miller and Miller 2002).

The root mean-square error (RMSE) was used to evaluate the differences between the experimental concentrations of the reactive species and the corresponding values of the proposed model. For 2,4-D, 2,4-DCP, HP, and Ox concentrations, the calculated RMSE were 3.61×10^{-2}, 5.91×10^{-3}, 2.16×10^{-1}, and 2.45×10^{-2} mM, respectively.

Firstly, it is important to note the strong influence of radiation on the process. For conditions of Fig. 2a (Tables 2 and 3, $N = 1$) where the concentration of HP employed was the lowest and q_{Tot}^{inc} maximum (also maximum $\Delta T^{120} = 14.1$ °C), the highest $X_{2,4\text{-}D}^{30}$ (79.7 %) was reached after 30 min. Also, for these conditions, the total destruction of the herbicide was attained in just 60 min of reaction ($X_{2,4\text{-}D}^{60} = 98.8$ %). Whereas for conditions of Fig. 2c (Tables 2 and 3, $N = 3$) where the q_{Tot}^{inc} was minimum, only $X_{2,4\text{-}D}^{30} = 57.3$ % were obtained. In addition, for $R = 28.5$, the herbicide conversions levels achieved were significant ($X_{2,4\text{-}D}^{30} = 78.6$ % and $X_{2,4\text{-}D}^{60} = 100$ %).

On the other hand, it is important to analyze the conversion levels achieved for TOC after 120 min of reaction. Here, the concentration of the oxidizing agent employed has an important role. For $R = 50$ and $R = 28.5$, the X_{TOC}^{120} obtained were 12.75 and 32.75 %, respectively, higher than that achieved for conditions of $R = 7$ (Table 2). Note that for $t = 120$ min, HP consumption associated with this test has been close to 95 %. Consequently, the concentration of the oxidizing agent remaining in the system is too low to achieve a higher level of mineralization.

The bioassay Microtox® was applied (see Fig. 3) in order to study the toxicity evolution of the system for conditions of run N=2 and N=3 (Table 3). At the initial time, a similar percentage of luminescence inhibition was observed (45.50 % for run N=2 and 44.25 % for run N=3). At this point, the toxicity is attributed to the presence of 2,4-D and ferrioxalate. The maximum level of inhibition was observed between $t = 15$ min and $t = 30$ min (50 and 75 % of inhibition), which is related to the appearance of 2,4-DCP in the system. For conditions of $R = 28.5$, the residual percentage of inhibition at 120 min is 8.05 %, which is in accordance with the disappearance of 2,4-D at 60 min and destruction of

Table 3 UV and total radiation levels experimentally measured and estimated

Nº	R	ΔT^{120} (°C)	q_{UV}^{exp} (W m^{-2})	q_{UV}^{est} (W m^{-2})	q_{Tot}^{exp} (W m^{-2})	q_{Tot}^{est} (W m^{-2})	q_{Tot}^{inc} (E cm^{-2} s^{-1})
1	7	14.1	39.6	38.5	1098.5	1078.8	1.26×10^{-7}
2	28.5	11.3	35.5	35.2	970.7	987.6	9.92×10^{-8}
3	50	9.4	30.1	31.4	825.2	834.8	7.72×10^{-8}

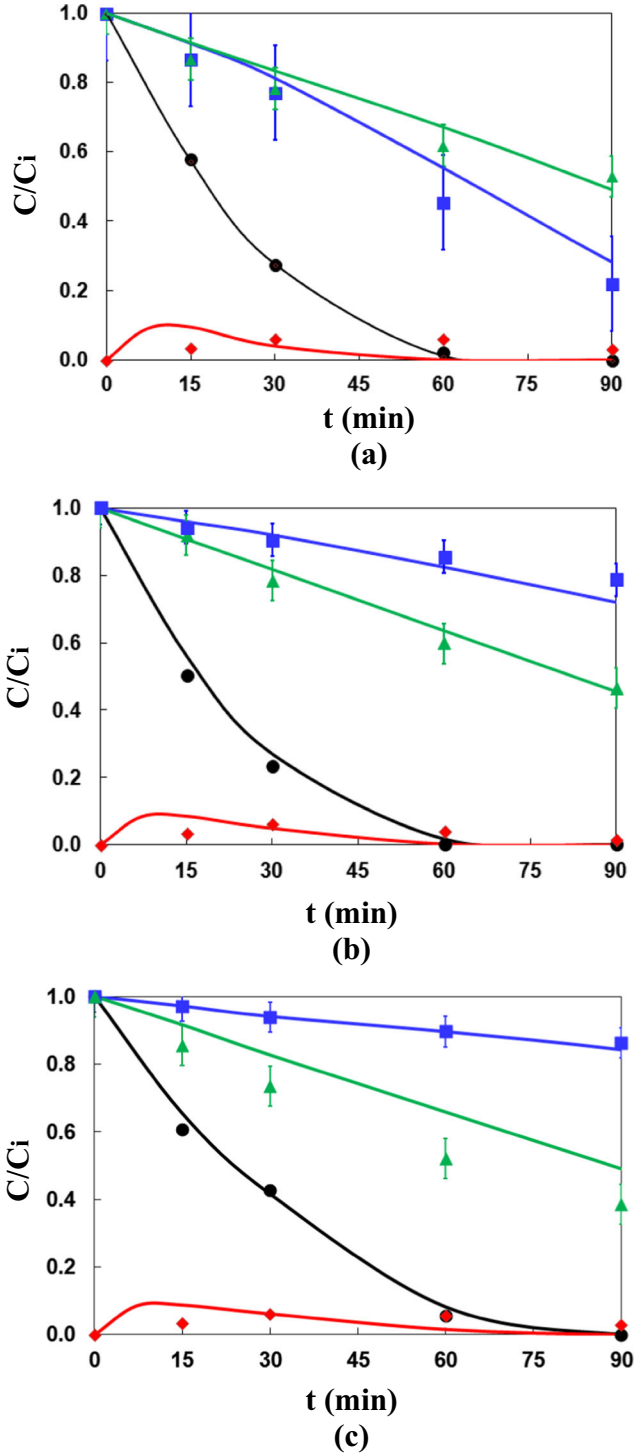

Fig. 2 Predicted (*solid line*) and experimental (*symbol*) relative concentrations versus time, for $C^0_{2,4\text{-D}} = 0.13$mM; $C^0_{C_2O_4^{2-}} = 0.54$mM and $C^0_{Fe^{3+}} = 0.054$mM. (**a**) $R = 7$; $Ta = 35$ °C. (**b**) $R = 28.5$; $Ta = 33$ °C. (**c**) $R = 50$; $Ta = 30$ °C. *Symbols*: 2,4-D (*black circle*), 2,4-DCP (*red diamond*), HP(*blue square*) and $C_2O_4^{2-}$(*green triangle*)

2,4-DCP at 120 min. In the case of the experiment carried out using a higher concentration of oxidizing agent ($R = 50$), the inhibition percentage begins to decrease with respect to the initial inhibition at 90 min (27.71 %), reaching a value of 18.50 % at 120 min. This residual toxicity could be also attributed to other compounds present in solution along with 2,4-DCP. Thus, formation of other intermediates during the herbicide degradation, such as chlorohydroquinones or chlorobenzoquinones, should receive larger attention.

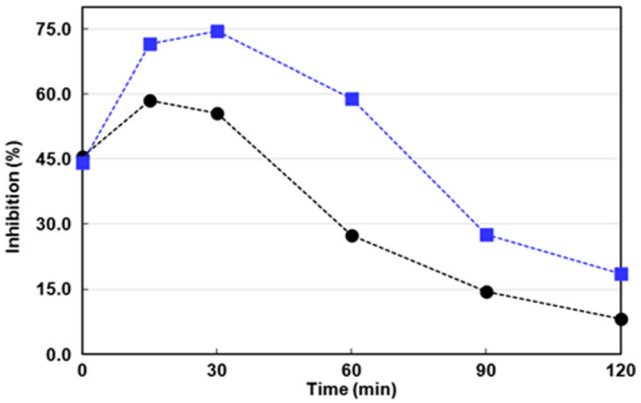

Fig. 3 Percentage of luminescence inhibition versus time. Keys: $R = 28.5$ (*black circle*) and $R = 50$ (*blue square*)

Conclusions

The solar photo-Fenton degradation of the herbicide 2,4-D at pH close to natural conditions was evaluated using ferrioxalate complex as the iron source. Here, a kinetic model validated in a previous contribution was used to predict the reactant concentrations during the oxidation process in a pilot-plant solar reactor.

The influence of the irradiation level, temperature (T), and hydrogen peroxide to 2,4-D initial concentration ratio (R) on the photo-Fenton process was also investigated. For a low concentration of hydrogen peroxide (HP) and maximum incident radiation (also maximum $\Delta T^{120} = 14.1$ ºC), the highest $X^{30}_{2,4\text{-D}}$ (79.7 %) was reached after 30 min. However, for these conditions, the X^{120}_{TOC} was only about 55.6 %. Note that for $t = 120$ min, HP consumption has been close to 95 %. In addition, for $R = 28.5$, the herbicide conversions levels achieved were significant ($X^{30}_{2,4\text{-D}} = 78.6$ % and $X^{60}_{2,4\text{-D}} = 100$ %).

It was shown that T and R strongly influence the herbicide conversion percentage. In the case of the reaction temperature, better degradation results were obtained when the highest values of T were reached. Furthermore, the pilot-plant solar reactor took advantage of the IR portion of solar energy, which heated the solutions without any additional cost. On the other hand, an intermediate level of the oxidizing agent concentration should be chosen; it was found that R must be higher than the stoichiometric value, but an excess of HP could produce a scavenging effect, reducing the catalytic activity.

For $R = 28.5$, the residual percentage of inhibition at 120 min was only 8.05 %. However, for $R = 50$ ($X^{30}_{2,4\text{-D}} = 57.3\,\%$ and $X^{60}_{2,4\text{-D}} = 91.5\,\%$), the residual percentage of inhibition at 120 min was still higher (18.50 %). This residual toxicity could also be attributed to other compounds present in solution along with 2,4-DCP.

Acknowledgments The authors are grateful to Universidad Nacional del Litoral (UNL), Consejo Nacional de Investigaciones Científicas y Técnicas (CONICET), and Agencia Nacional de Promoción Científica y Tecnológica (ANPCyT) for the financial support. They also thank Tec. Antonio C. Negro and Eng. Claudia Romani for their technical assistance.

References

Alfano MO, Bahnemann D, Cassano AE, Dillert D, Goslich R (2000) Photocatalysis in water environments using artificial and solar light. Catal Today 58:199–230

Alfano MO, Brandi RJ, Cassano AE (2001) Degradation kinetics of 2,4-D in water employing hydrogen peroxide and UV radiation. Chem Eng J 82:209–218

Bockelmann D, Weichgrebe D, Goslich R, Bahnemann D (1995) Concentrating versus non-concentrating reactors for solar water detoxification. Sol Energy Mater Sol Cells 38:441–451

Conte L, Farias J, Albizzati E, Alfano O (2012) Photo-Fenton degradation of the herbicide 2,4-dichlorophenoxyacetic acid in laboratory and solar pilot-plant reactors. Ind Eng Chem Res 51:4181–4191

Conte L, Querini P, Albizzati E, Alfano OM (2014) Photonic and quantum efficiencies for the homogeneous photo-Fenton degradation of herbicide 2,4-D using different iron complexes. J Chem Technol Biotechnol 89:1967–1974

Conte L, Schenone A, Alfano O (2016) Photo-Fenton degradation of the herbicide 2,4-D in aqueous medium at pH conditions close to neutrality. J Environ Manag 170:60–69

De Lima Perini J, Perez-Moya M, Pupo Nogueira R (2013) Photo-Fenton degradation kinetics of low ciprofloxacin concentration using different iron sources and pH. J Photochem Photobiol A 259:53–58

De Souza D, Trovó A, Antoniosi N, Silva M, Machado A (2013) Degradation of the commercial herbicide glyphosate by photo-Fenton process: evaluation of kinetic parameters and toxicity. J Braz Chem Soc 24:1451–1460

Farias J, Albizzati ED, Alfano OM (2010) New pilot-plant photo-Fenton solar reactor for water decontamination. Ind Eng Chem Res 49: 1265–1273

Hislop K, Bolton J (1999) The photochemical generation of hydroxyl radicals in the UV-vis/ferrioxalate/H_2O_2 system. Environ Sci Technol 33:3119–3126

Klamerth N, Malato S, Maldonado MI, Agüera A, Fernández-Alba AR (2010) Application of photo-Fenton as a tertiary treatment of emerging contaminants in municipal wastewater. Environ Sci Technol 44: 1792–1798

Kwan CY, Chu W (2004) A study of the reaction mechanisms of the degradation of 2,4-dichlorophenoxyacetic acid by oxalate-mediated photooxidation. Water Res 38:421–4221

Lucas MS, Peres JA, Amor C, Prieto-Rodríguez L, Maldonado MI, Malato S (2012) Tertiary treatment of pulp mill wastewater by solar photo-Fenton. J Hazard Mater 225–226:173–181

Malato S, Fernández-Ibañez P, Maldonado MI, Blanco J, Gernjak W (2009) Decontamination and disinfection of water by solar photocatalysis: recent overview and trends. Catal Today 147:1–59

Miller JN, Miller JC (2002) Statistics and chemometrics for analytical chemistry. Pearson-Prentice Hall, New York, USA

Miralles-Cuevas S, Oller I, Sánchez Pérez JA, Malato S (2015) Application of solar photo-Fenton at circumneutral pH to nanofiltration concentrates for removal of pharmaceuticals in MWTP effluents. Environ Sci Pollut Res 22:846–855

Monteagudo JM, Durán A, San Martín I, Aguirre M (2009) Effect of continuous addition of H2O2 and air injection on ferrioxalate-assisted solar photo-Fenton degradation of orange II. Appl Catal B Environ 89:510–518

Murov S, Carmichael I, Hug G (1993) Handbook of photochemistry, 2nd edn. Marcel Dekker, New York, pp 299–305

Nascimento CA, Teixeira AC, Guardani R, Quina FH, Chiavone-Filho O, Braun AM (2007) Industrial wastewater treatment by photochemical processes based on solar energy. J Sol Energy Eng 129:45–52

Navarro S, Fenoll J, Vela N, Ruiz E, Navarro G (2011) Removal of ten pesticides from leaching water at pilot plant scale by photo-Fenton treatment. Chem Eng J 167:42–49

Ollis DF (1991) Solar-assisted photocatalysis for water purification: issues, data, questions. In: Pelizzetti, Schiavello (eds) Photochemical conversion and storage of solar energy. Springer, Netherlands, pp 593–622

Parra S, Malato S, Blanco J, Péringer P, Pulgarin C (2001) Concentrating versus non-concentrating reactors for solar photocatalytic degradation of p-nitrotoluene-o-sulfonic acid. Water Sci Technol 44:219–227

Pérez M, Torrades F, Domènech X, Peral J (2002) Fenton and photo-Fenton oxidation of textile effluents. Water Res 36:2703–2710

Pignatello JJ, Oliveros E, MacKay A (2006) Advanced oxidation processes for organic contaminant destruction based on the Fenton reaction and related chemistry. Crit Rev Environ Sci Technol 36:1–84

Radjenovic J, Sirtori C, Petrovic M, Barcelo D, Malato S (2009) Solar photocatalytic degradation of persistent pharmaceuticals at pilot-scale: kinetics and characterization of major intermediate products. Appl Catal B: Environ 89:255–264

Schenone AV, Conte LO, Botta MA, Alfano OM (2015) Modeling and optimization of photo-Fenton degradation of 2,4-D using ferrioxalate complex and response surface methodology (RSM). J Environ Manag 155:177–183

Siegel R, Howell JR (2002) Thermal radiation heat transfer, 4th edn. Taylor & Francis, Washington, DC

Soares PA, Batalha M, Guelli Souza S, Boaventura RAR, Vilar VJP (2015) Enhancement of a solar photo-Fenton reaction with ferric-organic ligands for the treatment of acrylic-textile dyeing wastewater. J Environ Manag 152:120–131